IEEE Photonics Journal
An IEEE Photonics Society Publication

Open Access

Photonic Generation and Transmission of Dual-Band Dual-Chirp Microwave Waveforms at C-Band and X-Band With Elimination of Power Fading

Volume 13, Number 1, February 2021

Lu Wang
Tengfei Hao
Guangyi Li
Wenhui Sun
Ming Li
Ninghua Zhu
Wei Li

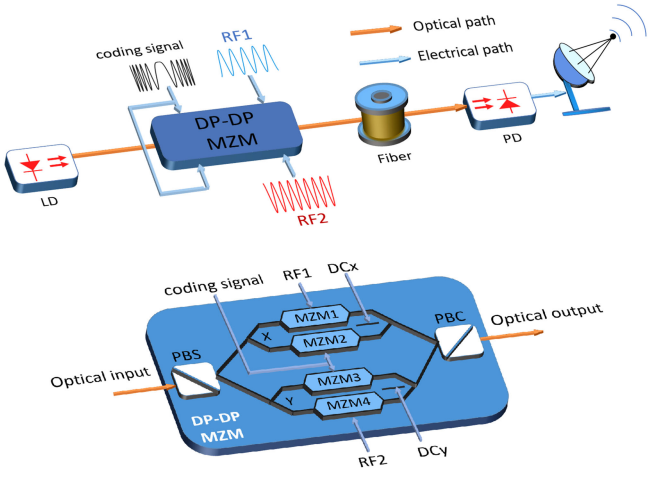

DOI: 10.1109/JPHOT.2021.3050254

Photonic Generation and Transmission of Dual-Band Dual-Chirp Microwave Waveforms at C-Band and X-Band With Elimination of Power Fading

Lu Wang,[1,2,3] Tengfei Hao,[1,2,3] Guangyi Li,[1,2,3] Wenhui Sun,[1] Ming Li,[1,2,3] Ninghua Zhu,[1,2,3] and Wei Li[1,2,3]

[1]State Key Laboratory on Integrated Optoelectronics, Institute of Semiconductors, Chinese Academy of Sciences, Beijing 100083, China
[2]School of Electronic, Electrical and Communication Engineering, University of Chinese Academy of Sciences, Beijing 100049, China
[3]Center of Materials Science and Optoelectronics Engineering, University of Chinese Academy of Sciences, Beijing 100190, China

DOI:10.1109/JPHOT.2021.3050254

Manuscript received December 8, 2020; revised December 25, 2020; accepted January 5, 2021. Date of publication January 8, 2021; date of current version January 22, 2021. This work was supported in part by the National Key Research and Development Program of China under Grant 2019YFB2203200, and in part by the National Natural Science Foundation of China (NSFC) under Grant 62075210, Grant 61620106013, and Grant 61835010. Corresponding author: Wei Li (e-mail: liwei05@semi.ac.cn).

Abstract: We propose a photonic method to generate and transmit dual-band dual-chirp microwave waveforms based on a dual-polarization dual-parallel Mach-Zehnder modulator (DP-DPMZM). The key novelty of this work is the generation of dual-band dual-chirp waveforms with flexible central frequency relationship to meet the requirement of the dual-band radar system, and transmission of the generated waveforms with elimination of power fading. In the proposed method, dual-band dual-chirp microwave waveforms are generated by applying two different RF signals and a parabolic coding signal to the DP-DPMZM. By properly adjusting the DC biases of the *x*-DPMZM and *y*-DPMZM, dispersion-induced power fading effect in the transmission of the generated waveforms can be compensated. A proof-of-concept experiment is conducted to generate and transmit dual-band dual-chirp microwave signals at C-band and X-band (centered at 7 GHz and 10 GHz) with tunable bandwidth. The proposed system has a simple structure and good reconfigurability, which has great potential in applications such as dual-band radar systems.

Index Terms: Microwave photonics, dual-band dual-chirp, pulse compression.

1. Introduction

Chirped microwave signals play a significant role in radar systems and are usually used to increase the pulse compression ratio and range resolution [1]. Conventionally, chirped microwave signals are generated by electrical links, which have limitations such as low frequency and small bandwidth. Thanks to the advantages of microwave photonics, chirped microwave signals have been widely generated by using photonic techniques with high frequency, large bandwidth, low loss, and immunity to electromagnetic interference [2], [3].

Generally, the generated chirped microwave signals are in single-band. In addition to the generation of single-band chirped microwave signals, the generation of multi-band chirped microwave

signals have also attracted lots of attentions due to their great potential in multi-band radar systems. Compared with single-band radars, the performance of multi-band radars on small target track, stealth target detection and multiple target separation can be enhanced simultaneously, since the multi-band radars works in more than one frequency bands [4]–[6]. Several microwave photonic methods have been proposed in recent years to generate multi-band chirped microwave signals. For example, the use of a polarization-division multiplexing dual-parallel Mach-Zehnder modulator (DPMZM) was proposed in [7] to generate two frequency-quadrupling chirped signals in two different bands. In this scheme, two 90° hybrid couplers are needed, which limit the bandwidth and frequency range of the generated microwave signals. In [8], two coherent optical frequency combs (OFCs) are introduced as multi-frequency optical local oscillators, where one of the two combs is modulated by an intermediate-frequency chirped signal. Chirped signals with flexible center frequencies can be obtained. However, the system contains two OFCs, which makes it complex and bulky.

On the other hand, dual-chirp microwave signals consist of two complementarily chirped microwave waveforms with opposite frequency chirping have also been widely considered in radar systems, since the range-Doppler coupling effect can be eliminated with the help of the arrival times of the two complementarily chirped microwave waveforms [9]–[11]. Dual-chirp microwave signals can also be generated using photonic methods. For example, a photonic method to generate frequency-doubling and bandwidth-quadrupling, or frequency-quadrupling and bandwidth-octupling dual-chirp microwave signals was reported in [12] based on high-order optical sidebands modulation using a dual-polarization dual-parallel Mach-Zehnder modulator (DP-DPMZM), but the generated signals were at single-band. Dual-band dual-chirp microwave waveforms with frequency-quadrupling and frequency-doubling or frequency-tripling and frequency-fundamental were generated by using high-order sideband modulation with different biases point of the modulator [13]. The system is simple, but the frequencies of the generated signals have the fixed multiple factor relationship. Dual-band dual-chirp waveforms can also be generated by using OFC as the input optical signal [14], [15]. In these schemes, a multi-wavelength light source or an additional modulator was used to generate the required OFC. In [16], [17], a polarization-division multiplexing modulator was used to generate the OFC and load a baseband chirped signal at the orthogonal polarization states. The above mentioned OFC-based method can generate multi-band dual-chirp microwave signals thanks to the large number of the comb lines of the OFC. However, a high power RF signal is needed in [16], [17] to generate the OFC, which leads to high power consumption. In addition, dual-chirp signals generated by double sideband modulation suffer from periodical power fading due to the chromatic dispersion in long distance fiber transmission [18]. In [17], single sideband modulation was used to overcome the power fading effect by using a 90° hybrid coupler, but the frequency range of the generated chirped waveforms was restricted by the 90° hybrid coupler. Moreover, the frequency intervals of the generated dual-chirp waveforms in different bands in the above mentioned methods are determined by the frequency spacing of the OFC, which have the fixed multiple factor relationship between different bands. Thus, it impedes flexible tuning of the center frequencies of the generated dual-chirp waveforms.

In this paper, we propose a photonic scheme to generate and transmit dual-band dual-chirp microwave signals at C-band and X-band with elimination of power fading by utilizing a dual-polarization dual-parallel Mach-Zehnder modulator (DP-DPMZM). The DP-DPMZM has a *x*-DPMZM and *y*-DPMZM with two orthogonal polarization states, and each sub-MZM is biased at the minimum transmission point (MITP) to realize carrier-suppressed modulation. Two different RF signals and a baseband parabolic coding signal are loaded to the DP-DPMZM, and the dual-band dual-chirp waveforms are generated after optical-to-electrical conversion. The power fading effect induced by chromatic dispersion can be compensated by adjusting the direct current (DC) biases of *x*-DPMZM and *y*-DPMZM. In this scheme, the center frequency of the generated dual-chirp microwave waveforms in different bands can be easily tuned to fulfill the needs of dual-band radar, which is hard to achieve based on conventional dual-band waveform generation schemes by using an optical frequency comb or high-order sideband modulation. The proposed scheme has good reconfigurability and simple structure, which can find potential applications in real-world scenarios.

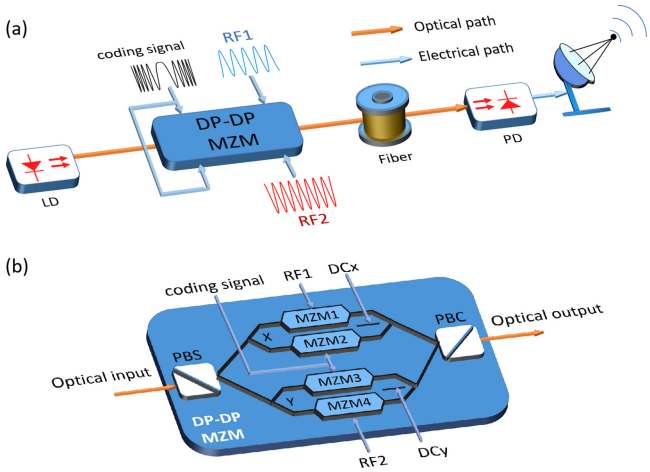

Fig. 1. (a) Schematic diagram of the proposed dual-band dual-chirp microwave waveform generation and transmission scheme. (b) Layout of the DP-DPMZM. LD, laser diode; DP-DPMZM, dual-polarization dual-parallel Mach-Zehnder modulator; PBS, polarization beam splitter; PBC, polarization beam combiner; PD, photodetector.

2. Principle

Fig. 1(a) shows the schematic configuration of the proposed dual-band dual-chirp microwave waveform generation and transmission system. A linearly polarized lightwave from a laser diode (LD) is injected into the DP-DPMZM. The layout of the DP-DPMZM is shown in Fig. 1(b), which has a polarization beam splitter (PBS), a polarization beam combiner (PBC), and two DPMZMs at orthogonal polarization states of *x* and *y*. Each DPMZM has two sub-MZMs. The baseband parabolic coding signal is divided by a power splitter and loaded on MZM2 and MZM3. At the same time, MZM1 at *x*-polarization state is driven by a microwave signal of RF1, while MZM4 at *y*-polarization state is driven by another microwave signal of RF2 with different frequency. Thus, the optical field at the output of the DP-DPMZM can be expressed as

$$\begin{bmatrix} E_{x1}(t) \\ E_{y1}(t) \end{bmatrix} = \frac{1}{4} A_0 e^{j\omega_0 t} \begin{bmatrix} \cos(m_1 \cos\omega_1 t + \frac{\phi_1}{2}) + \cos(m_2 \cos k(t - T/2)^2 + \frac{\phi_2}{2}) \cdot e^{j\phi_x} \\ \cos(m_4 \cos\omega_2 t + \frac{\phi_4}{2}) + \cos(m_3 \cos k(t - T/2)^2 + \frac{\phi_3}{2}) \cdot e^{j\phi_y} \end{bmatrix}, \quad (1)$$

where A_0 and ω_0 represent the amplitude and angular frequency of the optical carrier. ω_1 and ω_2 are the angular frequencies of RF1 and RF2, respectively. k and T represent the chirp rate and time duration of the baseband electrical coding signal, respectively. V_i, V_π and $m_i = \pi V_i / V_\pi$ ($i = 1$, 2, 3, 4) are the amplitude of electrical signal, half-wave voltage and modulation index, respectively. φ_i represents the DC phase shift of each sub-MZM, φ_x and φ_y are the corresponding DC phase shifts of x-DPMZM and y-DPMZM, respectively. By setting $\varphi_i = \pi$ to bias all sub-MZMs to MITP, and applying the Jacobi-Anger expansion to (1), we get

$$\begin{bmatrix} E_{x1}(t) \\ E_{y1}(t) \end{bmatrix} = -\frac{1}{2} A_0 e^{j\omega_0 t} \begin{bmatrix} J_1(m_1)\cos\omega_1 t + J_1(m_2)\cos(k(t - T/2)^2) \cdot e^{j\varphi_x} \\ J_1(m_4)\cos\omega_2 t + J_1(m_3)\cos(k(t - T/2)^2) \cdot e^{j\varphi_y} \end{bmatrix}. \quad (2)$$

The orthogonal polarized optical signals are combined by the PBC inside the DP-DPMZM. The combined optical signal is then sent to a photodetector (PD) to carry out optical-to-electrical conversion. The output photocurrent can be written as

$$\begin{aligned} i(t) &= E_{x1}(t) \cdot E_{x1}^*(t) + E_{y1}(t) \cdot E_{y1}^*(t) \\ &= \frac{1}{8} A_0^2 J_1^2(m_1)(1 + \cos 2\omega_1 t) + \frac{1}{8} A_0^2 J_1^2(m_2)(1 + \cos(2k(t - T/2)^2) \end{aligned}$$

$$+\frac{1}{4}A_0^2J_1(m_1)J_1(m_2)\cos\phi_x\cdot[\cos(\omega_1 t+k(t-T/2)^2)+\cos(\omega_1 t-k(t-T/2)^2)]$$
$$+\frac{1}{8}A_0^2J_1^2(m_4)(1+\cos 2\omega_2 t)+\frac{1}{8}A_0^2J_1^2(m_3)(1+\cos(2k(t-T/2)^2)$$
$$+\frac{1}{4}A_0^2J_1(m_3)J_1(m_4)\cos\phi_y\cdot[\cos(\omega_2 t+k(t-T/2)^2)+\cos(\omega_2 t-k(t-T/2)^2)]. \quad (3)$$

As can be seen from (3), dual-band dual-chirp microwave signals centered at ω_1 and ω_2 can be generated. The powers of the generated dual-chirp microwave signals at two bands can be adjusted separately by changing φ_{x} and φ_{y}. There also exist frequency-doubled and baseband signals, which can be easily eliminated by using an electrical bandpass filter.

When the output signal of the DP-DPMZM is transmitted through a long single mode fiber (SMF), the SMF dispersion would introduce phase shift to the optical signals. After fiber transmission, (2) can be rewritten as (4).

$$\begin{bmatrix}E_{x2}(t)\\E_{y2}(t)\end{bmatrix}=-\frac{1}{4}A_0e^{j\omega_0 t}\begin{bmatrix}J_1(m_1)(e^{j(\omega_1 t+\theta_{1,+1})}+e^{j(-\omega_1 t+\theta_{1,-1})})\\+J_1(m_2)(e^{j(k(t-T/2)^2+\theta_{1,0})}+e^{j(-k(t-T/2)^2+\theta_{1,0})})e^{j\phi_x}\\J_1(m_4)(e^{j(\omega_2 t+\theta_{2,+1})}+e^{j(-\omega_2 t+\theta_{2,-1})})\\+J_1(m_3)(e^{j(k(t-T/2)^2+\theta_{2,0})}+e^{j(-k(t-T/2)^2+\theta_{2,0})})\cdot e^{j\phi_y}\end{bmatrix}, \quad (4)$$

where $\theta_{\mathrm{i},0}$, $\theta_{\mathrm{i},+1}$ and $\theta_{\mathrm{i},-1}$ are the dispersion-induced phase shifts to the optical carrier and $\pm1^{\mathrm{st}}$ sidebands for $\mathrm{RF_n}$ ($n=1$ or 2), respectively. They can be expressed as

$$\begin{aligned}\theta_{i,0}&=z\beta(\omega_0)\\\theta_{l,+1}&=z\beta(\omega_0)+z\beta'(\omega_0)\omega_i+\tfrac{1}{2}z\beta''(\omega_0)\omega_i^2\\\theta_{i,-1}&=z\beta(\omega_0)-z\beta'(\omega_0)\omega_i+\tfrac{1}{2}z\beta''(\omega_0)\omega_i^2,\end{aligned} \quad (5)$$

where β, β' and β'' are the zeroth-order, first-order and second-order derivatives of the propagation constant β, respectively. z represents the transmission distance. In this case, the generated dual-band dual-chirp microwave waveforms after long fiber transmission can be rewritten as

$$\begin{aligned}i(t)&=E_{x2}(t)\cdot E_{x2}^*(t)+E_{y2}(t)\cdot E_{y2}^*(t)\\&=\frac{1}{8}A_0^2J_1^2(m_1)(1+\cos 2(\omega_1 t-\tau_0\omega_1))+\frac{1}{8}A_0^2J_1^2(m_2)(1+\cos(2k(t-T/2)^2)\\&\quad+\frac{1}{4}A_0^2J_1(m_1)J_1(m_2)\cos\left(\phi_x+\frac{zD\lambda_0^2\omega_1^2}{4\pi c}\right)\cdot\cos(\omega_1 t+k(t-T/2)^2+\tau_0\omega_1)\\&\quad+\frac{1}{4}A_0^2J_1(m_1)J_1(m_2)\cos\left(\phi_x+\frac{zD\lambda_0^2\omega_1^2}{4\pi c}\right)\cdot\cos(\omega_1 t-k(t-T/2)^2+\tau_0\omega_1)\\&\quad+\frac{1}{8}A_0^2J_1^2(m_4)(1+\cos 2(\omega_2 t-\tau_0\omega_2))+\frac{1}{8}A_0^2J_1^2(m_3)(1+\cos(2k(t-T/2)^2)\\&\quad+\frac{1}{4}A_0^2J_1(m_3)J_1(m_4)\cos\left(\phi_y+\frac{zD\lambda_0^2\omega_2^2}{4\pi c}\right)\cdot\cos(\omega_2 t+k(t-T/2)^2+\tau_0\omega_2)\\&\quad+\frac{1}{4}A_0^2J_1(m_3)J_1(m_4)\cos\left(\phi_y+\frac{zD\lambda_0^2\omega_2^2}{4\pi c}\right)\cdot\cos(\omega_2 t-k(t-T/2)^2+\tau_0\omega_2),\end{aligned} \quad (6)$$

where $\tau_0=z\beta'(\omega_0)$ and $D=-2\pi c\beta''(\omega_0)/{\lambda_0}^2$ are the group delay and second-order dispersion coefficient, respectively. λ_0 is the wavelength of the optical carrier, and c represents the velocity of light in vacuum. From (6), we can see that the amplitudes of dual-band dual-chirp microwave signals are related to $\cos(\varphi_{\mathrm{x}}+zD{\lambda_0}^2{\omega_1}^2/4\pi c)$ at ω_1 and $\cos(\varphi_{\mathrm{y}}+zD{\lambda_0}^2{\omega_2}^2/4\pi c)$ at ω_2, which are determined not only by phase shift induced by chromatic dispersion of the optical fiber, but also by

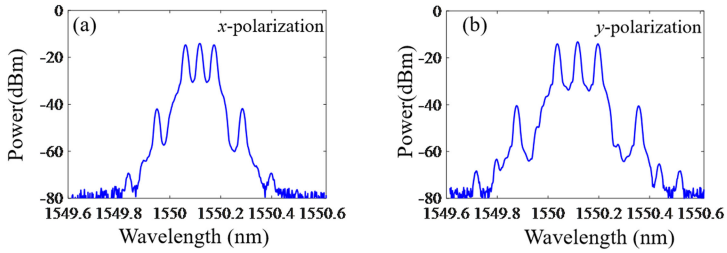

Fig. 2. (a) Optical spectrum of the signal at *x* polarization; (b) optical spectrum of the signal at *y* polarization.

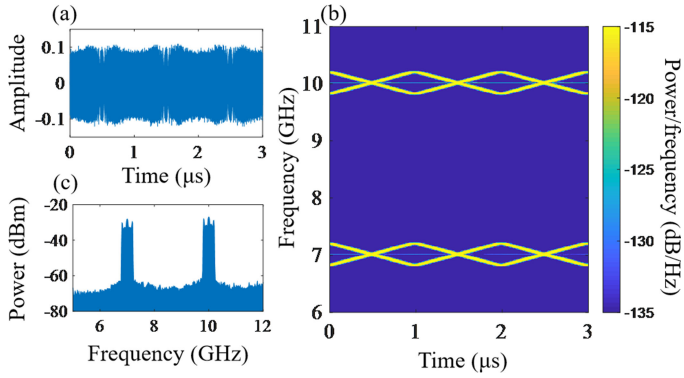

Fig. 3. (a) Temporal waveform, (b) instantaneous frequency-time diagram, and (c) electrical spectrum of the generated dual-band dual-chirp microwave signal with a bandwidth of 0.4 GHz.

the DC phase shift of *x*-DPMZM and *y*-DPMZM. Therefore, by properly setting the two DC phase shifts to make $\varphi_x + zD\lambda_0{}^2\omega_1{}^2/4\pi c = n_1\pi$ and $\varphi_y + zD\lambda_0{}^2\omega_2{}^2/4\pi c = n_2\pi$ (n_1 and n_2 are integer), the power of dual-band dual-chirp waveforms can be maximized. As a result, the power fading effect induced by chromatic dispersion can be compensated.

3. Results

An experiment based on the setup shown in Fig. 1(a) was performed. A linearly polarized lightwave at 1550.118 nm with power of 13 dBm was sent to the DP-DPMZM (Tektronix OM5110). The insertion loss of the DP-DPMZM is about 10.2 dB. An arbitrary waveform generator (Tektronix AWG 70001A) was used to generate the baseband parabolic coding signal with a bandwidth of 0.2 GHz and a time duration of 1μs. The generated baseband parabolic coding signal with power of -2 dBm was loaded on MZM2 and MZM3 with the help of a 3-dB power splitter. Two microwave sources (KEYSIGHT MXG Analog Signal Generator N5813B and ROHDE&SCHWARZ SMW200A, respectively) are used to generate RF signals to drive MZM1 and MZM4. The frequency of RF1 was 7 GHz, and the frequency of RF2 was 10 GHz, and the power of the two RF signals are both about 0 dBm. The four sub-MZMs of the DP-DPMZM were all biased at MITP to realize carrier-suppressed modulation. A PD (Agilent 11982A) with bandwidth of 15 GHz is used to carry out optical-to-electrical conversion. Fig. 2 shows the optical spectrum of the output optical field of the DP-DPMZM at *x* and *y* polarization states. The temporal waveform and corresponding instantaneous frequency-time diagram of the generated dual-band dual-chirp microwave signal are shown in Figs. 3(a) and 3(b), and the electrical spectrum is illustrated in Fig. 3(c). As can be seen, dual-band dual-chirp microwave signal is successfully generated with a bandwidth of 0.4 GHz and center frequencies of 7 GHz and 10 GHz, which have the potential to be used in radar systems at C-band and X-band. It should be noted that the generation of single-band dual-chirp microwave

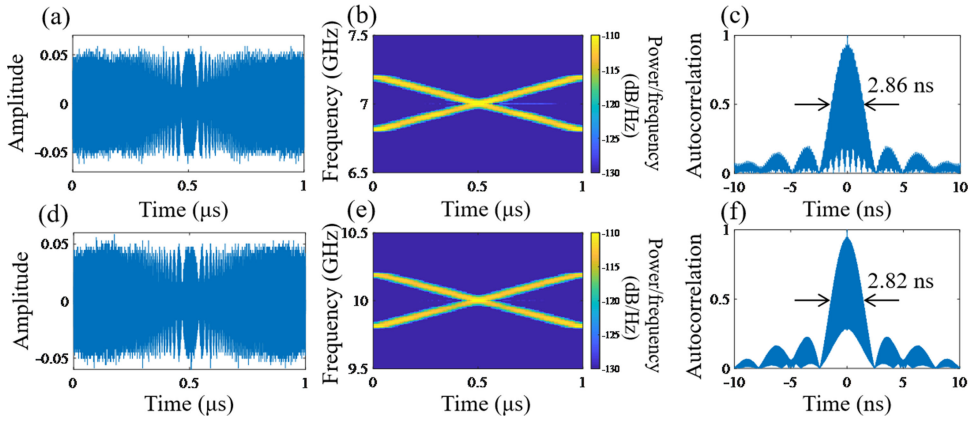

Fig. 4. (a) and (d) Temporal waveforms, (b) and (e) instantaneous frequency-time diagrams, (e) and (f) autocorrelation results of the filtered dual-chirp microwave signals with a bandwidth of 0.4 GHz and center frequencies of 7 GHz and 10 GHz, respectively.

waveforms based on a DPMZM has been proposed and demonstrated in [9]. In this paper, the dual-band dual-chirp waveforms is obtained and transmitted with the help of the commerical integrated DP-DPMZM, which consists of two discrete DPMZMs with a compact structure. The long fiber shown in Fig. 1(a) was removed in this case. Signal transmission in the long fiber will be discussed in later content of this paper. In order to demonstrate the pulse compression capability of the generated dual-band dual-chirp microwave signal, two electrical bandpass filters were used to select the microwave signals in the two bands. Figs. 4(a), 4(b) and 4(c) are the temporal waveform, instantaneous frequency-time diagram and autocorrelation result for the dual-chirp signal centered at 7 GHz, and Fig. 4(d), 4(e) and 4(f) are the temporal waveform, instantaneous frequency-time diagram and autocorrelation result for the dual-chirp signal centered at 10 GHz, respectively. The key parameters of autocorrelation include full width at half-maximum (FWHM) and the pulse compression ratio (PCR). The FWHMs are 2.86 ns and 2.82 ns for the two dual-chirp signals, respectively. The PCRs are defined as the ratio of the FWHM of the transmitted pulse to that of the compressed pulse, which are calculated to be 350 and 355, respectively. The PCRs for two bands are close to the theoretical time-bandwidth product (TBWP) of 400.

In order to show the reconfigurability of the proposed scheme, a dual-band dual-chirp microwave signal with a different bandwidth of 1 GHz was also generated, which can be easily achieved by changing the bandwidth of electrical parabolic coding signal. The experimental results are shown in Fig. 5 and Fig. 6. The FWHMs show in Fig. 6(c) and 6(f) are 1.16 ns and 1.2 ns for the two filtered dual-chirp signals, respectively. The corresponding PCRs are 862 and 833, which are consistent with the theoretical value. In addition, the center frequencies of the two dual-chirp microwave signals at the two bands depend only on the frequencies of the RF signals applied to DP-DPMZM, so the center frequencies are also tunable in the proposed system. Moreover, the proposed system also has the ability to generate multi-format microwave signals. For instance, a dual-band phase coded signal can be generated by changing the electrical parabolic coding signal to the 13-bit barker codes (or other codes with high-level '1' and low-level '−1'). Thus, the proposed system has a flexible reconfiguration.

The scheme proposed in this paper also has the function to eliminate the power fading effect induced by chromatic dispersion. In the transmission of single-band chirped microwave signal in previous work, the power fading effect can be eliminated, for example, by introducing a phase shift to the modulator. Here we demonstrate the feasibility of the use of this method to eliminate the power fading effect in the transmission of dual-band chirped microwave signal. Fig. 7 shows the simulation result of the power fading effect after 35-km SMF transmission for different RF frequencies in a traditional signal transmitter. It can be seen that there is a significant attenuation

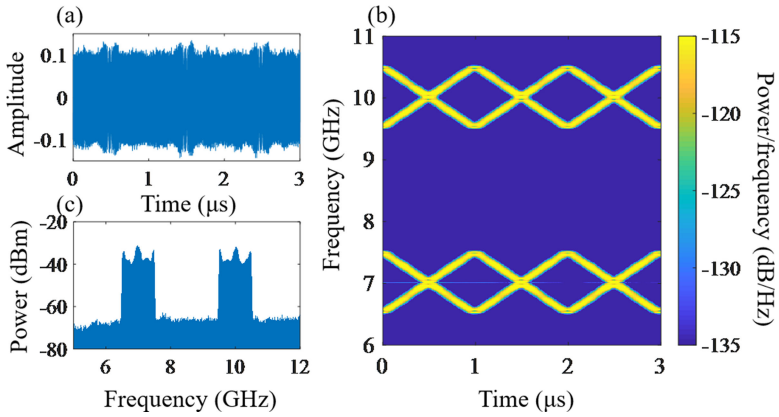

Fig. 5. (a) Temporal waveform, (b) instantaneous frequency-time diagram, and (c) electrical spectrum of the generated dual-band dual-chirp microwave signal with a bandwidth of 1 GHz.

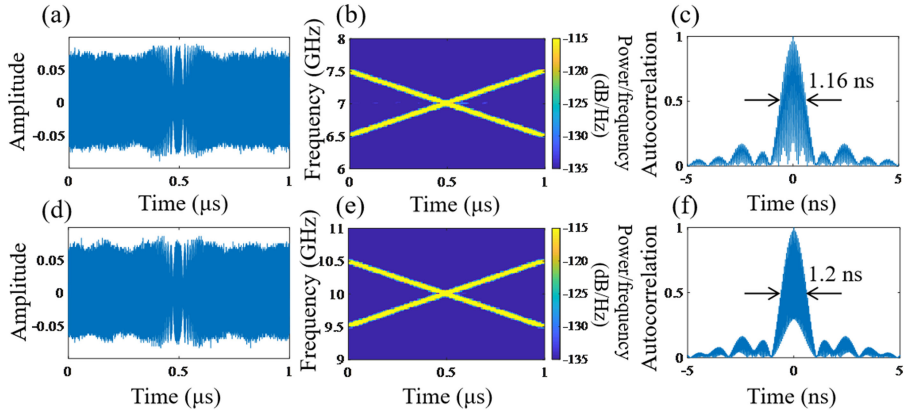

Fig. 6. (a) and (d) Temporal waveforms, (b) and (e) instantaneous frequency-time diagrams, (e) and (f) autocorrelation results of the filtered dual-chirp microwave signals with a bandwidth of 1 GHz and center frequencies of 7 GHz and 10 GHz, respectively.

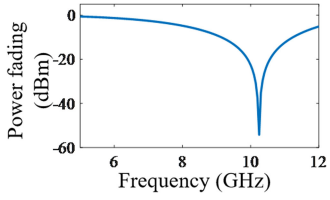

Fig. 7. Simulation result of the power fading effect after 35-km SMF transmission for different RF frequencies in a traditional signal transmitter.

at 10 GHz in such a transmitter. The transmission performance of the proposed system was experimentally evaluated by adding a SMF with the same length of 35-km to the optical link. The insertion loss of the used 35-km SMF in experiment is about 8 dB. In order to clearly show the performance of the elimination of power fading using the proposed system, a contrast experiment without SMF was also conducted by just adding a 8-dB optical attenuator, and the waveform, instantaneous frequency-time diagram, and electrical spectrum in this case are shown in Fig. 8(a), 8(b) and 8(c), respectively. As can be seen from Fig. 8(c), the powers of the center frequency components of the generated dual-band dual-chirp signals are both about −42 dBm. Fig. 8(d),

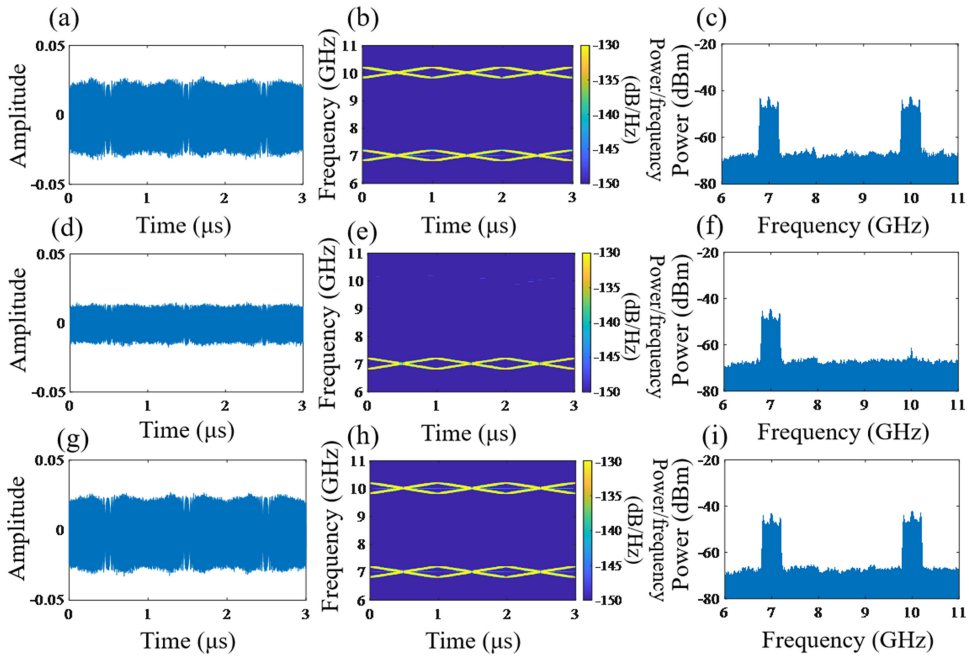

Fig. 8. (a), (b) and (c) waveform, instantaneous frequency-time diagram, and electrical spectrum of the dual-band dual-chirp microwave signals after optical attenuation in the contrast experiment; (b), (d) and (e) waveform, instantaneous frequency-time diagram, and electrical spectrum of the dual-band dual-chirp microwave signals after 35-km SMF transmission when the DC biases of the x-DPMZM and y-DPMZM are not unchanged; and (f), (g) and (h) waveform, instantaneous frequency-time diagram, and electrical spectrum of the dual-band dual-chirp microwave signals with compensation of the dispersion-induced power fading effect.

8(e) and 8(f) show the waveform, instantaneous frequency-time diagram and electrical spectrum of dual-band dual-chirp microwave signals after 35-km SMF transmission when the DC biases of the *x*-DPMZM and *y*-DPMZM are not changed. The powers of center frequency components of the two dual-chirp signals are attenuated to −44.3 dBm and −59.2 dBm, respectively. Obviously, there is a strong dispersion-induced power fading effect on the dual-chirp signal centered at 10 GHz. To overcome this issue, we adjusted the DC biases of the *x*-DPMZM and *y*-DPMZM to compensate the unwanted phase shifts induced by dispersion. The waveform, instantaneous frequency-time diagram and electrical spectrum after dispersion compensation are shown in Figs. 8(g), 8(h) and 8(i), respectively. The powers of the center frequency components are −42.8 dBm and −42 dBm for the two dual-chirp signals centered at 7 GHz and 10 GHz, respectively, which are similar with that of the contrast experiment where the long SMF is removed. Therefore, the transmission of the dual-band dual-chirp microwave signals with elimination of power fading is successfully demonstrated. It should be noted that there is a trade-off between large bandwidth TBWP and anti-chromatic dispersion transmission, since the power of the high components of the generated waveforms with large TBWP would be faded drastically due to the chromatic dispersion in the transmission process. We choose to generate dual-band dual-chirp waveforms with relative small TBWP in this paper in order to demonstrate the anti-chromatic dispersion transmission capability. Moreover, the OFC-based methods can also generate dual-band dual-chirp microwave waveform thanks to the large number of comb lines of the OFC. For OFC-based methods, the number of the RF source does not have to be equal to the number of the generated dual-chirp waveforms as in the proposed method, which saves the cost of the system. Although more microwave sources are needed in our scheme, the generated dual-band dual-chirp microwave waveforms have more flexible frequency relationship between different bands. The key novelty of this work is to generate

and transmit dual-band dual-chirp microwave waveforms with flexible frequency tuning ability, good reconfigurability and simple structure, which can find potential applications in real-world scenarios.

4. Conclusion

In this paper, the generation and transmission of dual-band dual-chirp microwave waveforms at C-band and X-band with elimination of power fading are theoretically analyzed and experimentally demonstrated. The proposed scheme can generate dual-band dual-chirp microwave signals with flexible central frequency relationship to satisfy the requirements of dual-band radar system, and the bandwidth and coding pattern of the generated signals can also be easily tuned. The proposed scheme has good reconfigurability and simple structure, which can find potential applications in real-world scenarios.

References

[1] W. Li, L. X. Wang, M. Li, H. Wang, and N. H. Zhu, "Photonics generation of binary phase-coded microwave signals with large frequency tunability using a dual-parallel mach-zehnder modulator," *IEEE Photon. J.*, vol. 5, no. 4, Aug. 2013, Art. no. 5501507.
[2] J. Yao, "Microwave photonics," *J. Lightw. Technol.*, vol. 27, no. 3, pp. 314–335, Feb. 2009.
[3] J. Capmany and D. Novak, "Microwave photonics combines two worlds," *Nat. Photon.*, vol. 1, no. 6, pp. 319–330, Jun. 2007.
[4] J. Tian, J. Sun, G. Wang, Y. Wang, and W. Tan, "Multiband radar signal coherent fusion processing with IAA and apFFT," *IEEE Signal Process. Lett.*, vol. 20, no. 5, pp. 463–466, May 2013.
[5] J. Han and C. Nguyen, "Development of a tunable multiband UWB radar sensor and its applications to subsurface sensing," *IEEE Sensors J.*, vol. 7, no. 1, pp. 51–58, Jan. 2007.
[6] P. Ghelfi, F. Laghezza, F. Scotti, D. Onori, and A. Bogoni, "Photonics for radars operating on multiple coherent band," *J. Lightw. Technol.*, vol. 34, no. 2, pp. 500–507, Jan. 2016.
[7] Q. S. Guo, F. Z. Zhang, P. Zhou, and S. L. Pan, "Dual-Band LFM signal generation by optical frequency quadrupling and polarization multiplexing," *IEEE Photon. Tech. Lett.*, vol. 29, no. 16, pp. 1320–1323, Aug. 2017.
[8] W. J. Chen, D. Zhu, C. X. Xie, T. Zhou, X. Zhong, and S. L. Pan, "Photonics-based reconfigurable multi-band linearly frequency-modulated signal generation," *Opt. Express*, vol. 26, no. 25, pp. 32491–32499, Dec. 2018.
[9] D. Zhu and J. Yao, "Dual-chirp microwave waveform generation using a dual-parallel mach-zehnder modulator," *IEEE Photon. Technol. Lett.*, vol. 27, no. 13, pp. 1410–1413, Jul. 2015.
[10] T. F. Hao, J. Tang, N. N. Shi, W. Li, N. H. Zhu, and M. Li, "Dual-chirp fourier domain mode-locked optoelectronic oscillator," *Opt. Lett.*, vol. 44, no. 8, pp. 1912–1915, Apr. 2019.
[11] G. Y. Li, L. Wang, S. Zhu, M. Li, N. H. Zhu, and W. Li, "Photonic generation of dual-chirp microwave waveforms based on a tunable optoelectronic oscillator," *IEEE Photon. Technol. Lett.*, vol. 32, no. 10, pp. 599–602, May 2020.
[12] X. Li, S. H. Zhao, Z. H. Zhu, K. Qu, T. Lin, and D. P. Hu, "Photonic generation of frequency and bandwidth multiplying dual-chirp microwave waveform," *IEEE Photon. J.*, vol. 9, no. 3, Jun. 2017, Art. no. 7104014.
[13] K. Zhang *et al.*, "Photonic approach to dual-band dual-chirp microwave waveform generation with multiplying central frequency and bandwidth," *Opt. Commun.*, vol. 437, pp. 17–26, Dec. 2019.
[14] K. Zhang, S. Zhao, T. Lin, X. Li, W. Jiang, and G. Wang, "Photonic generation of multi-frequency dual-chirp microwave waveform with multiplying bandwidth," *Results Phys.*, vol. 13, Jun. 2019, Art. no. 102226.
[15] K. Zhang *et al.*, "Photonic-based dual-chirp microwave waveforms generation with multi-carrier frequency and large time-bandwidth product," *Opt. Commun.*, vol. 474, May 2020, Art. no. 126076.
[16] L. Wang *et al.*, "Photonic generation of multiband and multi-format microwave signals based on a single modulator," *Opt. Lett.*, vol. 45, no. 22, pp. 6190–6193, Nov. 2020.
[17] K. Zhang *et al.*, "Photonics-based multi-band linearly frequency modulated signal generation and anti-chromatic dispersion transmission," *Opt. Express*, vol. 28, no. 6, pp. 8350–8362, Mar. 2020.
[18] S. Zhu, M. Li, N. H. Zhu, and W. Li, "Transmission of dual-chirp microwave waveform over fiber with compensation of dispersion-induced power fading," *Opt. Lett.*, vol. 43, no. 11, pp. 2466–2469, Jun. 2018.